40th AIAA Plasmadynamics and Lasers Conference
22 - 25 June 2009, San Antonio, Texas

AIAA 2009-4222

Aero-Optic Measurements Using a Laser-Induced Air Breakdown Beacon

R. Mark Rennie[1], Garnett Cross.[2]
Center for Flow Physics and Control
University of Notre Dame, Notre Dame, IN, 46556

David Goorskey[3], Matthew R. Whiteley[4]
MZA Associates Corporation, Dayton, OH, 45459

David Cavalieri[5], *and* Eric J. Jumper[6]
Center for Flow Physics and Control
University of Notre Dame, Notre Dame, IN, 46556

An experimental investigation into the optical behavior of a laser-induced air breakdown spark is described. The investigation concentrates on qualities of the air-breakdown spark, particularly the non-point-source character of the spark, that have a critical influence on the accuracy with which aero-optic aberrations can be measured using the return light from the spark. Data are presented that show that the spark dimensions conform to established physical models, and baseline spark wavefront noise figures are presented as a function of the optical system parameters. Wavefront measurements are shown that indicate that a well-designed beacon system should be capable of accurately measuring aero-optic aberrations created by realistic compressible shear-layer flows.

Nomenclature

D_C	=	aperture of spark-collimating lens
D_L	=	beam diameter at focusing lens
E	=	laser beam pulse energy
f_C	=	focal length of spark-collimating lens
f_L	=	focal length of laser-focusing lens
I	=	irradiance
OPD	=	optical path difference
St	=	Strehl ratio
Δt	=	laser beam pulse duration
w_0	=	beam waist diameter
λ	=	wavelength
ρ	=	density

I. Introduction

High field-of-regard, aircraft-mounted laser systems typically include parts of the operating envelope in which the laser must pass through highly-turbulent flow regions such as a turbulent boundary layer or a shear layer associated with a separated flow region. At subsonic and higher flight speeds, these turbulent flow regions become optically active such that a transiting laser beam will be distorted due to index-of-refraction variations within the

[1]Research Assistant Professor, Department of Aerospace and Mechanical Engineering, Senior Member AIAA.
[2]Graduate Research Assistant, Department of Aerospace and Mechanical Engineering, Student Member AIAA.
[3]Scientist, MZA Dayton Operations.
[4]Vice-President, Senior Scientist, MZA Dayton Operations, Member AIAA.
[5]Research Specialist, Department of Aerospace and Mechanical Engineering, Member AIAA.
[6]Professor, Department of Aerospace and Mechanical Engineering, Fellow AIAA.

flow [1-3] thereby degrading its on-target irradiance distribution. The study of the optical aberrations produced by compressible nearfield turbulent flows is called "aero-optics."

The phase characteristics of the initial light beam can be restored using an adaptive-optic (AO) system [4] that places the conjugate waveform of the aberration onto the optical wavefront of the beam prior to its transmission through the aberrating flowfield. In this case, the conjugate waveform must be determined from measurements of the aero-optic aberrations, which requires some kind of light source such as the reflected glint from the target or a natural or man-made guide star [5]. Even for feed-forward AO correction schemes, in which flow-control techniques are used to improve the frequency bandwidth of the aberrating flow, it is anticipated that low-order optical measurements will still be used to synchronize the AO scheme with the controlled flow aberrations [6, 7].

In practice, a man-made guide star could be generated by focusing a high-energy pulsed laser at a point outside the aircraft, thereby creating an air-breakdown spark with sufficient brightness for aero-optic measurements. The operational advantages offered by this kind of man-made guide star are significant since it can be placed at any point in space outside the aircraft. In [8], we described our experimental measurements of the aero-optic aberrations of a compressible shear layer using an artificial guide star that was simulated using the diverging light from an optical fiber. In these tests, anisoplanatism effects were evaluated by comparing wavefront aberrations from the fiber-optical point-source "beacon" to those from a collimated reference laser beam after passing through the compressible shear-layer flow; these measurements showed that it was possible to use the aberrations measured with the point-source beacon to accurately predict the aero-optic aberrations on the reference beam, despite the fact that the point-source beacon wavefronts had significant initial curvature and that the light from the point source sampled only a part of the aberrating flowfield through which the reference beam passed. Although the results of these initial tests were promising, it was noted that the light output from the optical fiber used to simulate the beacon had better optical properties than can be expected from a spark. In particular, the optical fiber used to create the diverging, simulated beacon had a core diameter of only 3.6 μm, so that the light from the fiber behaved effectively as a point source; in comparison, laser-induced breakdown sparks have sizes on the order of a few millimeters or larger [9]. Furthermore, the size and effective location of laser-induced breakdown sparks can fluctuate between pulses of the driving laser, while the effective origin of the light from the optical fiber could be held stationary. The next step in our investigation of an aero-optic beacon was therefore to evaluate the effects of the non-point-source optical character of laser-induced breakdown sparks, and to demonstrate the viability of the aero-optic measurements of [8] using an actual laser-generated beacon; this paper documents the approach and results of this investigation.

II. Characterization of the Air-Breakdown Beacon

A schematic of a generic aero-optic beacon system is shown in Fig. 1. A laser beam is focused using a lens with f-number = f_L/D_L to create a breakdown spark, and the return light from the beacon is imprinted with the aberrations imposed by an intervening optically-active flow. The beacon light is then collimated using a lens with f-number = f_C/D_C after which it is directed on to a wavefront-measurement instrument. For an operational system, working values for f_L/D_L, f_C/D_C will likely be at least 10, and have a practical upper limit of around 40. The system shown in Fig. 1 is very simplified and ignores many other design parameters that can affect the beacon system performance; however, it will be shown that the effect of the non-point-source behavior of the spark is determined primarily by the values f_L/D_L, f_C/D_C.

A. Laser Breakdown Effects

The waist diameter of a focused laser beam is given by [10]:

$$w_0 = \frac{4\,\lambda\, f_L}{\pi\, D_L} \qquad (1)$$

The average irradiance at the spot location for a beam with pulse energy E and pulse duration Δt is therefore:

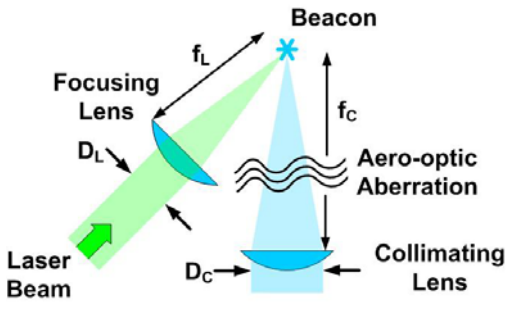

Fig. 1. Generic aero-optic beacon system.

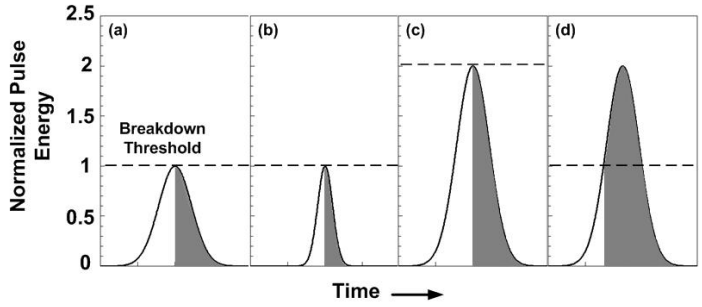

Fig. 2. Fraction of laser pulse energy absorbed by spark (shaded) for (a) baseline pulse shape, (b) shorter pulse duration, (c) higher pulse energy required to achieve breakdown, and (d) pulse energy that exceeds breakdown threshold.

$$I = \frac{E}{4\,\pi\,\Delta t \left(\frac{\lambda\, f_{\mathrm{L}}}{\pi\, D_{\mathrm{L}}} \right)^2} \tag{2}$$

Breakdown and spark formation occurs when the irradiance at the waist location exceeds the breakdown threshold of the ambient gas.

Equation (2) shows that the ability of a particular laser to achieve breakdown depends strongly on the emission wavelength and the pulse duration of the laser. Measurements [11-13] also show that the breakdown threshold varies with wavelength by several orders of magnitude, but that the threshold is lower at infra-red ($\lambda \approx 1$ μm) and ultra-violet ($\lambda \approx 350$ nm) wavelengths.

When the focused laser irradiance exceeds the gas breakdown threshold, atoms in the gas become ionized by the large electric field strength in the focal region, and the return of these atoms back to the ground state is accompanied by the emission of secondary light. At the most common test pressures and laser wavelengths, the dominant mechanism of gas ionization is cascade ionization (inverse bremsstrahlung), although multi-photon ionization may become important at high altitudes (eg. ~30,000 ft) where the gas pressure is significantly lower and if shorter (UV) laser wavelengths are used [14, 15]. After breakdown is achieved, the gas at the breakdown location becomes effectively opaque to the laser radiation and absorbs practically all of the energy in the latter part of the laser pulse [15]. Figure 2 shows schematically the portion of the laser pulse that is absorbed for different cases, and illustrates how the energy input into the breakdown spark is affected by pulse duration (Fig. 2(b)), or by factors that increase the pulse energy required for breakdown (Fig. 2(c)), specifically, as shown by Eq. (2), a larger breakdown threshold, longer wavelength or large f_L/D_L. If the laser pulse energy is greater than the level required to achieve breakdown, then the additional energy is also absorbed by the breakdown spark, as shown in Fig. 2(d).

The breakdown spark grows rapidly to a size that is several orders of magnitude larger than the focal region of the initiating laser beam. In particular, the breakdown spark tends to grow back towards the focusing lens within the solid angle containing the incident laser beam. The spark growth has been well modeled as a radiation-driven detonation wave [9, 16 – 19], with a front velocity given by

$$v = \left[\frac{2\,(\gamma^2 - 1)\,E_A}{\pi\,\Delta t\,\rho_2\,x^2\,\tan^2\alpha} \right]^{1/3} \tag{3}$$

where E_A is the energy absorbed, as shown approximately in Fig. 2. In Eq. (3), ρ_2 is the air density behind the shock front:

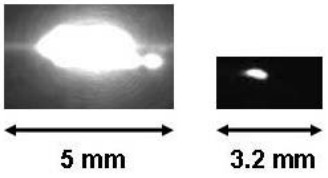

Figure 3. High-speed camera images of sparks created using (left) λ = 1.06 μm, E = 135 mJ, f_L/D_L = 12.5 and (right) λ = 355 nm, E = 6 mJ, f_L/D_L = 15 (sea level pressure).

$$\rho_2 = \rho_1 \left(\frac{\gamma + 1}{\gamma} \right) \tag{4}$$

where ρ_1 is the initial air density. Assuming a square pulse shape, Eq. (3) can be integrated to give the growth of the luminous front, or visible spark length:

$$x = (5/3)^{3/5} \left[\frac{2\,(\gamma^2 - 1)\,E_A}{\pi\,\Delta t\,\rho_2\,\tan^2\alpha} \right]^{1/5} t^{3/5} \tag{5}$$

Note that in Eqs. (3) and (5), α is the half angle of the focused incident laser beam; as such:

$$\frac{1}{\tan\alpha} = \frac{f_L}{D_L} \tag{6}$$

More realistic solutions for the spark length computed, for example, for a Gaussian shaped laser pulse, can be found in [17]; however, the essential result is that the spark length scales with the absorbed pulse energy and f_L/D_L of the focusing lens. The scaling of spark length with pulse energy is illustrated in Fig. 3, which shows high-speed photographic images of laser-induced breakdown sparks created using a YAG laser emitting at 1.06 μm and at 355 nm, and shows that the much larger input energies required for spark formation in the IR result in substantially larger sparks than can be achieved at UV wavelengths.

In practice, the size of the spark can also vary from pulse to pulse, presumably due to small variations in the conditions affecting the formation of the spark. The resulting spark length fluctuations are likely a result of variations in the amount of energy absorbed by the spark; for example, in [15] a variation in the effective breakdown threshold of ± 15% is reported which, as shown in Fig. 2, would result in significant variations in the absorbed energy. From Eq. (5), the sensitivity of the spark length to fluctuations in the absorbed energy is given by

$$\frac{\mathrm{d}x}{\mathrm{d}E_A} = 0.272\left[\frac{2(\gamma^2-1)}{\pi\,\Delta t\,\rho_2\,E_A{}^4}\left(\frac{f_L}{D_L}\right)^2\right]^{1/5} t^{3/5} \tag{7}$$

where Eq. (6) has been used for tan α. Equation (7) shows that the amount of pulse-to-pulse length variation is also larger for more narrowly-converging laser beams focused using large f_L/D_L.

Large spark sizes, and particularly large variations in the spark size that result in a motion of the effective spark location, can interact with the optical system used to collimate the spark light for wavefront measurements, creating spurious noise on the spark wavefronts which can interfere with the measurement of aero-optic aberrations. This effect highlights the importance of using the smallest sized spark that satisfies the brightness requirements of the wavefront-measuring optical system. As shown in this section, small spark sizes are achieved by employing a small f_L/D_L, as well as using small laser pulse energies which, as shown by Eq.(2), can be achieved by using short pulse durations and short laser wavelengths as well as, again, a small f_L/D_L ratio.

B. Beacon Optical Characterization

The above considerations point to the use of YAG lasers for aero-optic beacon formation. Commercially-available versions of this laser typically have considerably shorter pulse durations than other types of lasers, around 5 ns. Furthermore, although the fundamental emission of the YAG is at 1.06 μm, frequency-tripled versions have an output wavelength of 355 nm. The comparatively short pulse duration and wavelength of the frequency-tripled YAG results in smaller pulse energies required for breakdown with concomitant smaller breakdown spark dimensions.

Based on this, a "Brilliant" Nd-YAG laser with triple-harmonic generator (THG) package (Δt = 5 ns, λ = 355 nm) manufactured by Quantel Inc. was selected for beacon formation. The maximum pulse energy of the laser is 100 mJ, which is more than adequate to achieve breakdown at cruise altitudes up to 30,000 ft [11, 12]. The pulse repetition frequency of the laser is fixed at 10 Hz. This pulse rate is probably too slow to capture the development of most aero-optic flows, which typically have bandwidths on the order of a few kilohertz; however, the 10 Hz pulse rate of the laser should be more than adequate for synchronization of an AO correction system with the "regularized" aero-optic aberrations that can be achieved using flow control as part of a feedforward AO correction strategy [6, 7].

1. High-Speed Camera Measurements

High-speed images of the breakdown spark were made using a Photron Fastcam SA1-1.1 monochrome high-speed imaging camera. The images were acquired at a frame rate of 5 x 10^5 images per second (2 μs per image). The camera was positioned to view the spark at right angles to the optical axis of the spark laser, so that the images showed the length and diameter of the sparks, which were roughly axi-symmetric in shape. Example images of the spark are shown in Fig. 3.

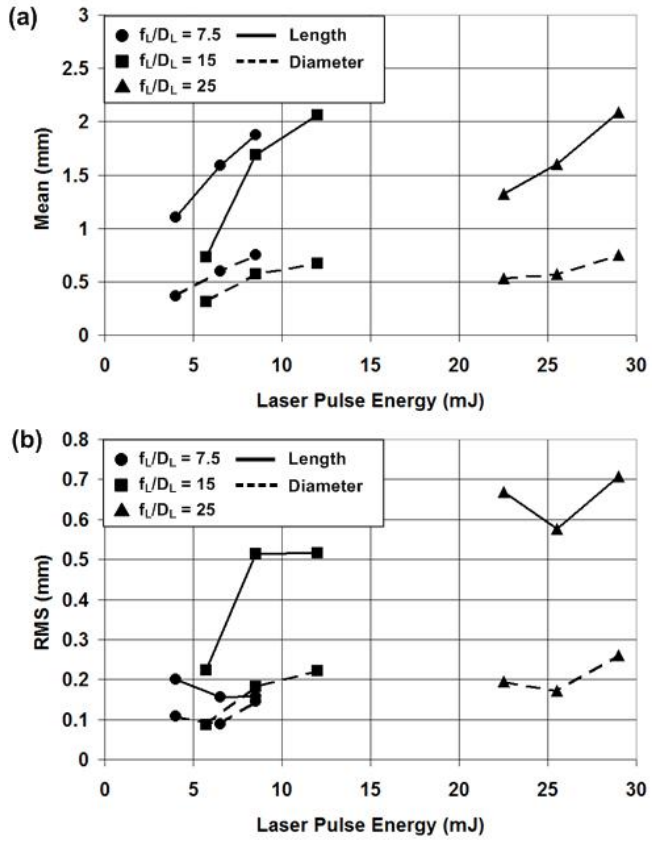

Figure 4. Spark dimensions from high-speed camera images

The mean and rms of the spark length and diameter, measured from the high-speed camera images, are summarized in Fig. 4. Figure 4(a) shows that the spark is generally much longer than its diameter, that the spark length increases with the pulse energy and that generally greater energies are required to generate the sparks as f_L/D_L increases; all of these trends agree with the predictions of Eqs. (2) to (6). Figure 4(b) shows that variations in the spark dimensions, particularly the rms of the spark length, increase with increasing f_L/D_L, in agreement with Eq. (7). It should be noted that, since a spherical lens was used to focus the laser, some of the variation in laser energy required to generate the sparks may have been due to spherical aberrations produced by the focusing lens; however, Fig. 4 generally conforms to the expected spark behavior outlined in Section A.

2. Spark Wavefront Measurements

Measurements of the spark wavefronts were made using the experimental setup shown in Fig. 5. The wavefront sensor was a Shack-Hartmann configuration with a 33 x 44 lenslet array manufactured by Wavefront Sciences. As shown in Fig. 5, there were no intervening aberrations between the breakdown spark and the wavefront sensor, so that the measured wavefronts show baseline aberrations produced by the spark and optical system. The wavefronts were acquired in a nearly backscatter arrangement; the 20° angle between the optical axes of the wavefront and laser beams was the minimum possible to avoid interference between the two sets of optical components.

The wavefront data were acquired in the form of optical path differences (OPD's) from the mean over the measurement aperture. These wavefront data were further processed by removing tip, tilt and piston, and by removing the mean wavefront of the data set. A plot of the root-mean-square of the OPD variations (i.e. OPD_{rms})

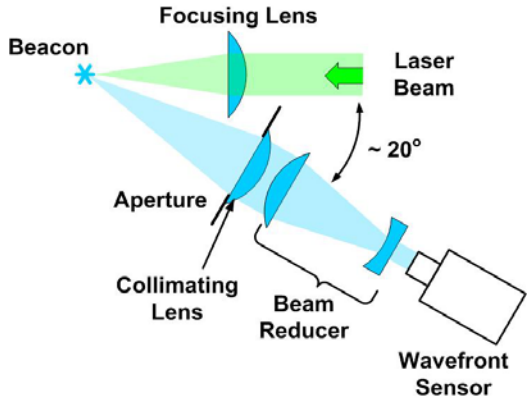

Figure 5. Optical setup for baseline beacon wavefront measurements.

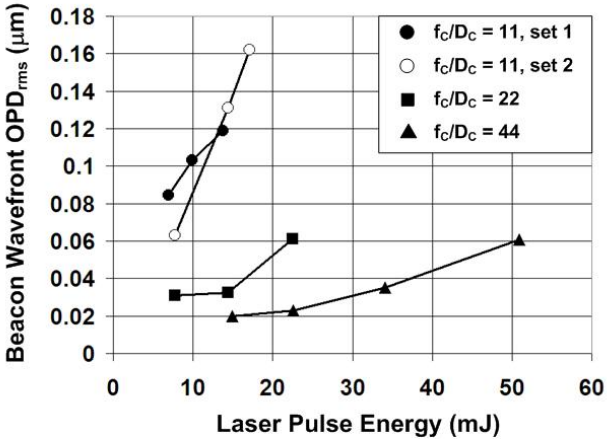

Figure 6. OPDrms of unaberrated beacon wavefront as a function of f/D of the collimating lens. f/D of lens used to focus the laser was f_L/D_L = 15.

over the measurement aperture as a function of the laser pulse energy is shown in Fig. 6 for different ratios of f_C/D_C of the lens used to collimate the light from the beacon. The figure shows that the OPD_{rms} of the baseline beacon wavefronts decreases significantly as f_C/D_C increases, and increases as the pulse energy increases for a given value of f_C/D_C.

Insight into the trends shown in Fig. 6 can be obtained by examining the rms of the OPD variations over the measurement aperture for a typical run, shown in Fig. 7. The large, circularly-shaped OPD variations around the center and edge of the aperture shown in Fig. 7 are characteristic of variations in the overall curvature, or "focus," of the spark wavefront, and are symptomatic of a fluctuation in the effective location of the spark towards or away from the collimating lens. Since the wavefront sensor viewed the spark nearly parallel to the optical axis of the driving UV laser beam, the focus variation in the spark wavefront was therefore likely caused by the variation in the effective location of the spark which, as discussed in Section A and shown in Fig. 4, is largest along the optical axis of the driving laser beam.

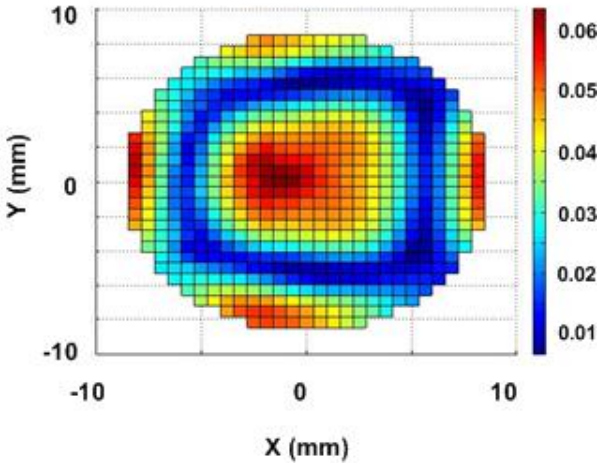

Figure 7. OPDrms (μm) over aperture for typical baseline beacon wavefront measurement.

Using simple lens theory [20], it can be shown that the OPD_{rms} caused by small deviations ε in the location of a point source toward or away from the focal point and along the optical axis of a lens with focal length f_C is given by:

$$\text{OPD}_{\text{rms}} = \frac{\varepsilon}{28\left(\frac{f_c}{D_c}\right)^2} \tag{8}$$

where D_C is the diameter of the aperture at the collimating lens. Using Eq.(8), the effective spark motion amplitude ε was computed for the data shown in Fig. 6; Fig. 8 shows that the resulting ε data, except for a few outliers, correlate well with the laser pulse energy. The positive correlation of ε with the laser pulse energy, as shown in Fig. 8, agrees with the results of the high-speed camera measurements shown in Fig. 4, and with Eq. (7). A linear curve fit to the computed ε data is:

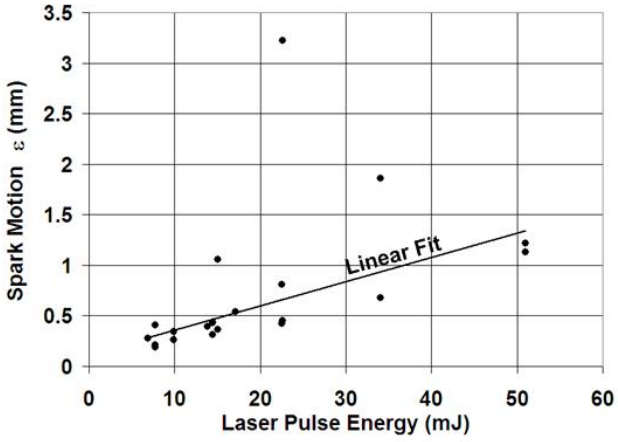

Figure 8. Apparent spark motion ε computed from OPDrms of baseline beacon vavefronts

$$\varepsilon = 0.0239\,E + 0.122 \tag{9}$$

where ε is in mm and E is in mJ. Substitution of Eq. (9) into Eq. (8) gives:

$$\text{OPD}_{\text{rms}} = \frac{0.854\,\text{E} + 4.34}{\left(\frac{f_c}{D_c}\right)^2} \quad (\text{Note: } f_L/D_L = 15) \tag{10}$$

The data of Fig. 6 are replotted with the fit of Eq. (10) in Fig. 9, which shows a good comparison between the fit and the data except for the $f_C/D_C = 44$ data (which appear as "outliers" in Fig. 8); it is likely that the OPD_{rms} for the $f_C/D_C = 44$ data is sufficiently small that the relative importance of other noise sources besides the spark motion increases, making Eq.(10) less accurate for this case.

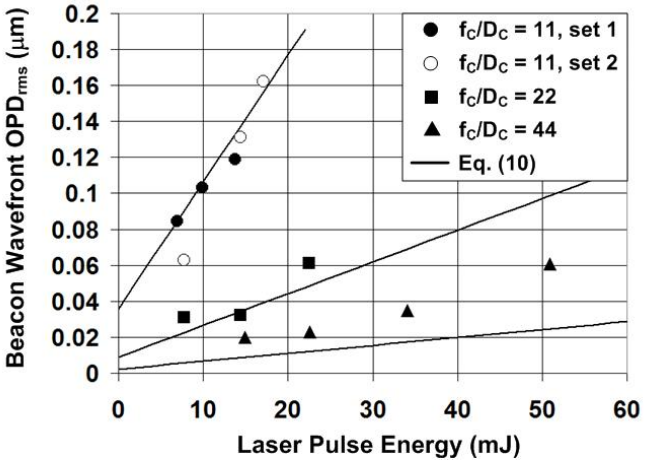

Figure 9. Comparison of focus model for baseline beacon aberrations, Eq. (10), with measured wavefronts.

3. Spark Brightness

Beacon optical data has been presented thus far as a function of the input laser pulse energy *E*. This method of presentation facilitates immediate comparison of the experimental results with relationships describing the physics of the breakdown spark, Eqs. (2) to (7). For the design of an operational aero-optic beacon system, however, design specifications are more likely to be placed on the beacon brightness required to achieve a satisfactory signal-to-noise ratio for the optical instrumentation, with the laser pulse energy being adjusted to whatever level generates this brightness.

The spark brightness was measured using a Newport model 842PE optical power meter with a model 918D-SL-003 photodiode-type photodetector. The photodiode-type detector is well suited for these measurements because of the high sensitivity of the detector; however, a drawback of the detector is that its sensitivity is wavelength dependent (although other types of detectors also exhibit various amounts of wavelength sensitivity). Spectral analysis of air breakdown sparks [21] shows that most of the visible light emitted from the plasma occurs at short wavelengths (violet/blue), and is associated with nitrogen emissions. As such, assuming violet/blue emission, and assuming isotropic radiation from the spark, the total optical energy radiated from the spark was determined to be approximately 0.24% of the excess input laser pulse energy above the breakdown threshold. This level of brightness was sufficient for accurate measurements using our wavefront sensor at laser energies down to or slightly greater than the breakdown threshold (~ 5 to 10 mJ/pulse), even for very large f_C/D_C (up to ~ 40) where the fraction of the total spark light captured by the optical system was very small.

4. Spark Lifetime

The spark lifetime has important implications on the usefulness of the spark for measuring aero-optic aberrations. In particular, a long spark lifetime would raise the possibility that the position or dimensions of the spark might be significantly distorted by convection effects if the spark were created in a high-speed flow. This kind of distortion of the spark would presumably also interact with the optical system used to measure the spark wavefronts, creating another source of spurious noise on the spark wavefronts in addition to the noise resulting from the normal spark dimension fluctuations discussed above.

The spark lifetime was measured using a FDS02 fast photodiode manufactured by Thorlabs. This photodiode is designed for telecommunications applications and has a nominal rise time of 47 ps. The measurements were made by focusing the spark light onto the photodiode using a 50 mm focal length lens. Figure 10 shows a phase-lock averaged oscilloscope trace of 16 spark emissions for a laser pulse energy of 45 mJ, and indicates that the majority of the light emitted from the spark is emitted within a 20 ns time period. This lifetime is significantly shorter than values reported in [22] (170 ns) and [23] (~ 90 ns); however, the breakdown sparks investigated in these studies were created using YAG lasers emitting at the fundamental (1064 nm) and first harmonic (532 nm), with longer pulse times, and using significantly greater pulse energies, so it is possible that the longer spark lifetimes reported in [22, 23] are a result of the different parameters of the driving laser beam.

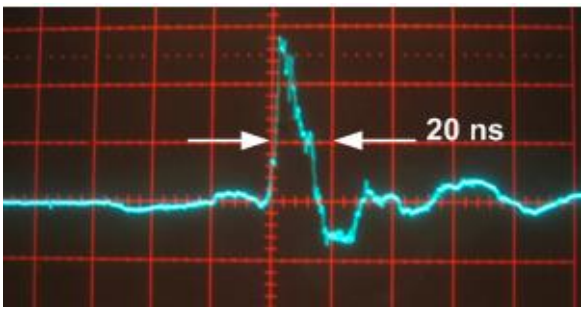

Figure 10. Oscilloscope time trace of emission from spark measured using fast photodiode.

The maximum distortion of the spark corresponds roughly to the flow convection distance over the spark lifetime. It is anticipated that the aero-optic beacon system will be deployed on aircraft that operate at subsonic

velocities. In this case, the 20 ns spark lifetime results in a convection distance on the order of a few micrometers even for flow speeds as high as Mach 1. This convection distance is orders of magnitude less than the normal fluctuations in spark dimensions shown in Fig. 4, indicating that the spark lifetime should have a negligible effect on the optical quality of the aero-optic beacon system.

III. Wavefront Measurements

The optical characterization of the laser breakdown spark presented in Section II has shown that the behavior of the spark conforms to established theory. Furthermore, the experimental data indicate that the noise levels on the spark wavefronts are caused primarily by fluctuations in the spark dimensions caused by spark-to-spark variations in the amount of absorbed energy, and baseline noise levels for the spark wavefronts in the absence of any intervening aberrations were measured, Fig. 6. The next step in the investigation was to test the accuracy with which aberrations with realistic amplitudes could be measured using the return light from the spark. It was decided to first investigate aberrations with OPD's corresponding to realistic compressible shear-layer flows, since these flows represent one of the most important types of aero-optic flows,.

Peak-to-peak, and rms OPD's measured in the University of Notre Dame Compressible Shear Layer Wind Tunnel (CSLWT) are summarized in Table 1. This wind tunnel mixes co-directional high- and low-speed flows at high subsonic flow speeds (up to Mach 1.0) to create a shear layer that is aero-optically active. As shown in [6, 24], the CSLWT flow and associated aberrations are representative of the kinds of aero-optic flows likely to be encountered on full-scale flight vehicles. Furthermore, the CSLWT shear-layer flow can be regularized using mechanical forcing that oscillates the trailing edge of the splitter between the high- and low-speed flows in a direction perpendicular to the flow direction, resulting in more regular, sinusoidal aero-optic aberrations. Table 1 shows that the peak-to-peak OPD of the aberrations in the CSLWT at a typical measurement distance of 400 mm downstream of the splitter trailing edge is approximately 1 μm and slightly greater when the shear layer is forced.

Parameter	Mean (μm)	Minimum (μm)	Maximum (μm)
Unforced OPD_{rms}	0.233	0.097	0.697
Unforced OPD_{PP}	1.119	0.567	2.563
Forced OPD_{rms}	0.291	0.1101	0.568
Forced OPD_{PP}	1.300	0.605	2.283

Table 1: Aero-optic aberrations measured in the Notre Dame Compressible Shear-Layer Wind Tunnel, at a distance x = 400 mm from the splitter [25]. The high-speed flow Mach number was 0.78 and the low-speed flow Mach number was 0.12.

The suitability of the spark for wavefront measurements was tested by placing stationary (non-moving) aberrations into the return light path from the spark. Using stationary aberrations allows testing of the aero-optic beacon system in a more controlled environment without the additional measurement noise due to vibrations that typically occur during measurements of moving aero-optic flows. The simulated, stationary aberrations used in the tests were selected to give OPD's similar to the levels associated with typical compressible shear-layer flows, Table 1. Through some trial and error, it was found that aberrations of a comparable amplitude could be produced by passing the light through a $1/16^{th}$-inch thick sample of plexiglas.

The optical setup used for the stationary aberration measurements is shown in Fig. 11. The spark was viewed in a backscatter arrangement at an angle of approximately 20^o to the optical axis of the UV laser beam. The plexiglas plate was placed in the optical path of the spark light and an aperture was placed on the collimating lens for the spark beam such that the diameter of the spark beam at the plexiglas aberration was approximately 17 mm. A 25 mm diameter reference beam was also passed through the plexiglas at the same location as the spark beam; the anisoplanatism [8] between the reference and spark measurements of the aberration therefore consisted of the difference in beam diameter and angle at the aberration, as well as the difference in wavefront shape at the aberration (spherical for the spark beam and planar for the reference beam).

Lens parameters for the optical setup were $f_L/D_L = 15$, $f_C/D_C = 24$, and the laser pulse energy was $E = 11$ mJ. The measured OPD_{rms} of the unaberrated spark wavefront was 0.036 μm, which closely agrees with the curve fit of Eq. (10). Peak-to-peak OPD variations on the unaberrated spark wavefront were approximately 0.2 μm, or around

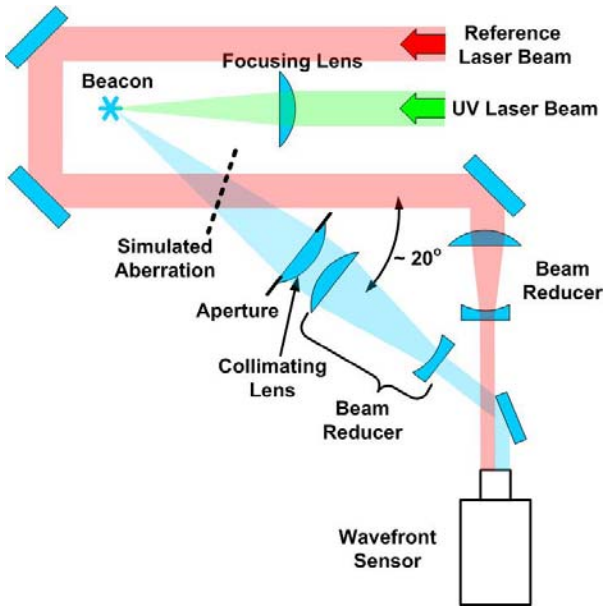

Fig. 11. Optical setup for stationary aberration measurements.

1/5th of the typical peak-to-peak shear-layer aberrations shown in Table 1. Using the large-aperture approximation for a nominal 1 μm wavelength,

$$St = \exp\left[-\left(\frac{2\pi \,\mathrm{OPD}_{\mathrm{rms}}}{\lambda}\right)^2\right] \tag{11}$$

the Strehl ratio, *St* (i.e. the ratio of on-axis beam energy to the optimum, diffraction-limited case), corresponding to the $\mathrm{OPD}_{\mathrm{rms}}$ of the unaberrated spark wavefront is 95%. This indicates that the baseline spark wavefront noise should not significantly impact the ability to measure the 1 μm peak-to-peak simulated aberration.

A sample of reference-beam and spark wavefronts for six different simulated aberrations is shown in Fig. 12. The figure shows that the plexiglas plate successfully produced aberration amplitudes in the range of Table 1. Furthermore, the aberrations measured by the spark (right side of each image) closely matched the aberration measured by the collimated reference beam, even without any corrections applied to the spark wavefronts to adjust for anisoplanatism effects [8]. The average cross-correlation value between the spark and collimated wavefronts, also without any corrections applied for anisoplanatism effects, was approximately 75%. It should be noted, however, that the worst cross-correlations between the two beams correspond to situations in which the spark beam happened to measure a region of the plexiglas plate over which the OPD variation was much smaller than the nominal 1 μm peak-to-peak variations that typically occur in shear-layer flows, so that the baseline spark wavefront noise had an unrealistically-large effect on the comparison between the two beams. For cases in which the spark beam measured peak-to-peak OPD's closer to 1 μm, the cross-correlation between the two beams was around 90%.

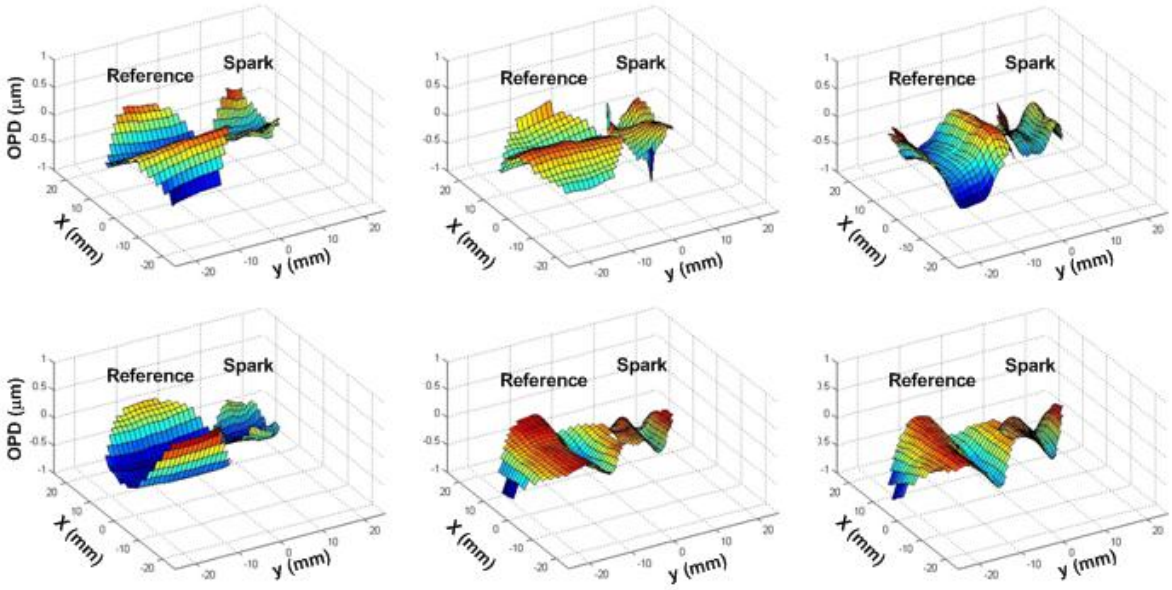

Fig. 12. Samples of wavefronts measured through 1/16th-inch thick plexiglas plate. Spark wavefront is shown on the right of each image.

IV. Discussion

The finite dimensions of the laser-induced air breakdown spark, and more importantly, the spark-to-spark variations in those dimensions, have significant impact on the ability to use the return light from the spark to measure aero-optic aberrations. This work has shown that the behavior of the spark size and shape conform to the established physics for the laser-breakdown process, and has produced experimentally-determined relationships describing the nature and magnitude of wavefront "noise" associated with the return light from the spark.

Based on the presented results, it is possible to note desirable features of an aero-optics beacon system that minimize the spark wavefront noise. In particular, spark dimensions and variations can be reduced by using a small value for f_L/D_L, as well as minimizing the required laser pulse energy which, as shown by Eq.(2), can be achieved by using short pulse durations and short laser wavelengths as well as, again, a small f_L/D_L ratio. Further, Eq. (10) shows that the effect of the non-point-source character of the spark can be mitigated by using a large value for f_C/D_C in the optical system used to measure the spark wavefronts. Many of these design features are critically linked to other system requirements, or cannot be independently fixed. For example, the laser pulse energy is also the primary factor affecting the spark brightness and hence the system signal level. Furthermore, although the spark noise is minimized by small f_L/D_L and large f_C/D_C values, a realistic optical design will likely have these values roughly the same. As such, design of an aero-optics beacon system will involve compromises, and a first estimate for the effect of the spark wavefront noise might be obtained using the large-aperture approximate, Eq. (11). For λ=1 μm radiation, Eq. (11) shows that an acceptable Strehl ratio of 90% is still obtained for OPD_{rms} up to 0.05 μm; as shown by Fig. 9, this limit on spark noise still leaves a considerable range of possibilities open to the optical designer and, as demonstrated by the stationary aberration measurements, it is possible to use the spark to measure aero-optic aberration magnitudes associated with realistic compressible shear-layer flows using a realistic optical setup.

Acknowledgments

These efforts were sponsored by the Air Force Research Laboratory Directed Energy Directorate under Contract Number FA9451-08-C-0100. The U.S. Government is authorized to reproduce and distribute reprints for governmental purposes notwithstanding any copyright notation thereon.

References

[1] Gordeyev, S., Post, M.L., McLaughlin, T., Ceniceros, J., and Jumper, E.J., "Survey of Optical Environment over Hemisphere-on-Cylinder Turret Using Suite of Wavefront Sensors," AIAA-2006-3074, June, 2006.

[2] Gordeyev, S., and Jumper, E.J., "Aero-Optical Characteristics of Compressible Subsonic Turbulent Boundary Layers," AIAA-2003-3606, June, 2003.

[3] Fitzgerald, E.J. and Jumper E.J., "The optical distortion mechanism in a nearly incompressible free shear layer," *Journal of Fluid Mechanics*, Vol. 512, 2004, pp. 153-189.

[4] Tyson, R.K., *Principles of Adaptive Optics*, Academic Press, Inc., San Diego, 1991.

[5] Whiteley, M.R., Welsh, B.M., and Roggemann, M.C., "Optimal modal wave-front compensation for anisoplanatism in adaptive optics," *J. Opt. Soc. Am. A*, **15**, no.8, Aug. 1998, pp 2097-2106.

[6] Rennie, R.M., Duffin, D.A., and Jumper, E. J., "Characterization and Aero-Optic Correction of a Forced Two-Dimensional, Weakly-Compressible Subsonic Free Shear Layer," *AIAA Journal*, November, 2008, pp.2787-2795.

[7] Nightingale, A.M, Duffin, D.A., Lemmon, M., Goodwine, B., and Jumper, E.J., "Adaptive-Optic Correction of a Regularized Compressible Shear Layer," AIAA 2006-3072, June, 2006.

[8] Rennie, R.M., Whiteley, M.R., Cross, G., Cavalieri, D., and Jumper, E.J., "Measurement of Beacon Anisoplanatism Through a Two-Dimensional Weakly-Compressible Shear Layer," AIAA-2008-4215, June, 2008.

[9] Ready, J.F., *Effects of High-Power Laser Radiation*, Academic Press, New York, 1971.

[10] Svelto, O., *Principles of Lasers*, Plenum Press, New York, 1998.

[11] Buscher, H.T., Tomlinson, R.G., and Damon, E.K., "Frequency Dependence of Optically Induced Air Breakdown," *Physical Review Letters*, Vol. 15, No. 22, Nov., 1965, pp 847 – 849.

[12] Turcu, I.C.E., Gower, M.C., and Huntington, P., "Measurement of KrF laser breakdown in gases," *Optics Communications*, Vol. 134, Jan. 1997, pp 66 – 68.

[13] Tran, P.X., and White, C.m., "Optical Characterization of the Laser-Induced Spark in Air," National Energy Technology Laboratory U.S. Department of Energy.

[14] Thiyagarajan, M. and Scharer, J.E. "Experimental Investigation of 193-nm Laser Breakdown in Air," *IEEE Transactions on Plasma Science*, Vol. 36, No. 5, Oct. 2008, pp. 2512-21.

[15] Chen, Y.L, Lewis, J.W.L., and Parigger, C., "Spatial and temporal profiles of pulsed laser-induced air plasma emission," *Journal of Quantitative Spectroscopy and Radiative Transfer*, Vol. 67, 2000, pp. 91-103.

[16] Ostrovskaya, G.V., and Zaidel, A.N., "Laser Spark in Gases," Sov. Phys.-Usp., vol. 16, No. 6, May, 1974, pp.834-855.

[17] Daiber, J.W., Thompson, H.M., "Laser-Driven Detonation Waves in Gases," *Physics of Fluids B*, Vol. 10, No. 6, June, 1967, pp. 1162-69.

[18] Jumper, E.J., "Transient Analysis of a Laser Supported Detonation Wave Using Whitham's Rule," *Physics of Fluids*, Vol. 21, April 1978, pp. 549-551.
[19] Jumper. E.J., "Implications of Applying a Global Energy Balance to Laser-Supported and Chemical Detonation Waves," *Physics of Fluids*, Vol. 27, Sep., 1984, pp. 2361-64.
[20] Klein, M.V., *Optics*, John Wiley and Sons, New York, 1970.
[21] Laux, C.O., Spence, T.G., Kruger, C.H., and Zare, R.N., "Optical diagnostics of atmospheric air plasmas," *Plasma Sources Science and Technology*, Vol. 12, 2003, pp. 125-138.
[22] Neal, D.R., et. al., "Wavefront sensor testing in hypersonic flows using a laser-spark guide star," *SPIE Journal*, Vol. 3172, pp. 347 – 359.
[23] Bindhu, C.V., et.al., "Energy absorption and propagation in laser-created sparks," *Applied Spectroscopy*, Vol. 58, No. 6, 2004, pp. 719-726.
[24] Rennie, R. M., Siegenthaler, J. P., and Jumper, E. J., "Forcing of a Two-Dimensional, Weakly-Compressible Subsonic Free Shear Layer," AIAA 2006-0561, Jan., 2006.
[25] Duffin, D.A., "Feedforward Adaptive-Optic Correction of a Weakly-Compressible High Subsonic Shear Layer," Ph.D.Dissertation, Dept. of Aerospace and Mechanical Engineering, Univ. of Notre Dame, Notre Dame, IN, 2009.